Temperature dependence of electron focusing in $In_{1-x}Ga_xAs/InP$ heterojunctions

J. Heremans, B. K. Fuller, C. M. Thrush, and D. L. Partin
Physics Department, General Motors Research and Development Center, Warren, Michigan 48090
(Received 20 January 1995)

Transverse electron focusing is studied in a two-dimensional electron gas in the lattice-matched $In_{1-x}Ga_xAs/InP$ system, as a function of temperature ($3\ K < T < 180\ K$) and areal electron density ($5\times10^{11}\ cm^{-2} < N_a < 9.5\times10^{11}\ cm^{-2}$). Focusing is observed up to temperatures above 100 K. The electron mean free path in this system is influenced by phonon scattering at temperatures above 30 K. The purpose of this study is to provide experimental data on the dependence of the amplitude of the focusing peak on temperature, along with mobility data in the same temperature range. The decay of the focusing peak amplitude with increasing temperature is not solely correlated with the reduction in electron relaxation time τ, as calculated from mobility. The results could possibly indicate a temperature dependence for the small-angle scattering. The energies involved in this focusing experiment scale as $\hbar/2\tau \approx kT < \hbar\omega_c$ at low temperature (4 K), while they scale as $\hbar/2\tau < \hbar\omega_c < kT$ at $T > 15$ K. This implies that thermal smearing of the Fermi surface is also important.

INTRODUCTION

When the geometrical length scale of a metal or semiconductor sample becomes comparable to the mean free path of the charge carriers in that system, transport in that sample occurs in what is known as the ballistic regime. In that regime, electrons or holes can be focused between an injecting contact and a collecting contact using a magnetic field. These phenomena have been observed in bismuth in different geometries since the 1960s,[1,2] and reviews of the work on semimetals and metals can be found in Refs. 3 and 4. Ballistic electron transport has later been observed in two-dimensional (2D) electron[5,6] and hole[7] systems in GaAs-$(Al_{1-x}Ga_x)As$ heterostructures by many authors. The most used geometry is called the transverse electron focusing (TEF) geometry, which is also used in this work. The experiment is set up as follows: two small contacts are placed on one side of a sample, at a distance L smaller than the electron mean free path. A constant current I is injected between one of these contacts, called the injector, by a bias voltage V_a between the injector and a third contact at the far side of the sample. A magnetic field is then applied perpendicularly to the sample plane. The second contact is the collector. For magnetic-field values such that the distance between emitter and collector equals the cyclotron orbit diameter, a maximum in the voltage V measured between the collector and the far contact is observed, if the Fermi surface has a circular cross section. Higher-order maxima are observed at higher fields, involving reflections of the charge carriers on the sample side. TEF experiments have been used to study the Fermi surfaces of solids,[8] and the interactions of charge carriers with the boundaries of the samples[4] and with phonons.[9]

The present work is a systematic study of the first-electron focusing-peak amplitude as a function of temperature. Its aim is to provide data over as wide a temperature range as possible, using a semiconductor system with narrower gap than GaAs, in which the high-temperature mobility is higher: the 2D electron gas in the lattice-matched $In_{1-x}Ga_xAs/InP$ system. Phonon scattering contributes to the electron mobility above 30K in this system. The devices have very small dimensions compared to those in previous work: the length scales are on the order of 1000 Å for the injector contact widths, and 3000–5000 Å for the distance L between injector and collector. This is larger than the extent of the Fermi wavelength λ_F (in our samples, $350\ Å > \lambda_F > 290\ Å$). Electron mean free paths calculated from mobility data, l_μ, range from 17 000 Å at liquid-helium temperatures to 5000 Å at 120 K, so that data can be obtained in the $T < 120$-K range. Only the amplitude of the lowest field focusing peak is studied, avoiding reflections of the electrons on the device edge.

EXPERIMENT

Four metal-organic chemical vapor deposition (MOCVD)-grown lattice-matched $In_{0.53}Ga_{0.47}As/InP$ samples are used in this study. The samples are labeled 539, 540, 541, and 542, and are doped differently. The sample profiles are InP substrate (Fe doped)/4000-Å undoped InP/y (Å) InP:Si $n = 1.0\times10^{18}\ cm^{-3}$/200-Å undoped InP/1000-Å $In_{1-x}Ga_xAs$. Electrons accumulate in a two-dimensional electron gas (2DEG) in the $In_{1-x}Ga_xAs$ at the InP interface. The effective mass of the electrons in $In_{0.53}Ga_{0.47}As$ is about $0.045m_e$, where m_e is the free-electron mass. The thickness (y) of the doped layer is varied in 60-Å steps, to increase the electron density in the active $In_{1-x}Ga_xAs$ region. Rectangular Hall bars are photolithographically defined in a sample of each growth, with a length-to-width ratio greater than 10:1 to avoid geometrical magnetoresistance effects, and measured in fields from $-1\ T < B < 1\ T$ at temperatures from 4.2 to 300 K. Samples 539 and 540 are also measured in the $-1\ T < B < 5\ T$ and $2.5\ K < T < 50\ K$ range, to analyze Shubnikov–de Haas (SdH) oscillations. A Fourier analysis of the latter gives an electron density

within 2% of the density obtained from low-field Hall data taken during the same cooldown on sample 539, and within 10% on sample 540. Only one sublevel is occupied. From cooldown to cooldown, the densities vary by less than 20%, while the mobilities remain within 6–8 %. The electron mobilities obtained from the low-field Hall measurements are shown as a function of temperature in Fig. 1. The electron densities in each of the four growths were essentially temperature independent below 100 K, and are also given in Fig. 1. From the areal density N_a and the mobility μ, the mobility mean free path l_μ can be calculated:

$$l_\mu = \hbar / e_\mu (2\pi N_a)^{1/2} . \quad (1)$$

From each growth, 1–4 transverse electron focusing devices are manufactured as mesas using electron-beam lithography and wet chemical etching. The nominal geometrical dimensions of the devices, obtained from scanning electron microscopy (SEM) micrographs, are given in Table I. The geometrical distance L_g between the center of the injector and the center of the collector contacts varies from 3000 to 5000 Å, while the width (W) of the injectors varies from 500 to 2000 Å. The electrical widths of the contacts, and the distance between them, can vary appreciably from the geometrical dimensions, because of the existence of a depletion layer around the sample edge.

The TEF samples are measured using a low-frequency ac resistance bridge (Linear Research LR 400) working at 15.9 Hz, using a bias voltage V_a varying from 0.02 to 0.2 mV, yielding currents of 10–100 nA. The bridge output is the ratio of the voltage V between the collector contact and the far contact to the excitation current I between the injector and the far contact. This quantity was measured in fields varying from −1 to 1 T, at temperatures ranging from liquid helium to 180 K. Experimental curves for three samples are shown in Figs. 2, 3, and 4, in which V/I is plotted as a function of field at various temperatures. Every sample tested from the four growths did show focusing, which, given our biasing conditions, shows up as a maximum in the V/I curves at $B > 0$. The field B_m at which a maximum in V/I is located is given in Table I, and should correspond to the field at which one-half electron cyclotron orbit fits between the emitter and the collector contacts:

TABLE I. Properties of the TEF devices. The sample number consists of the three-digit growth number (which corresponds to the numbers in Fig. 1) followed by a four- or five-digit device number. W is the estimated geometrical width of the injector and collector contacts, and L_g the geometrical distance between their centers. B_m is the field at which the maximum of the focusing peak is observed, and L_e is the electrical distance between contacts, as determined from Eq. (2).

Sample	W (Å)	L_g (Å)	B_m (T)	L_e (Å)
539-2125	2000	4000	0.675	3420
539-2127	800	4300	0.56	4130
540-2151	1200	3000	0.85	3030
540-2152	2000	3500	0.80	3200
540-2155	600	3500	0.82	3140
540-2156	1000	4300	0.685	3760
541-2098	2000	4000	0.68	4200
541-20911	2000	4000	0.657	4320
541-2172	700	5000	0.59	4800
542-2111	1000	4000	0.80	4000

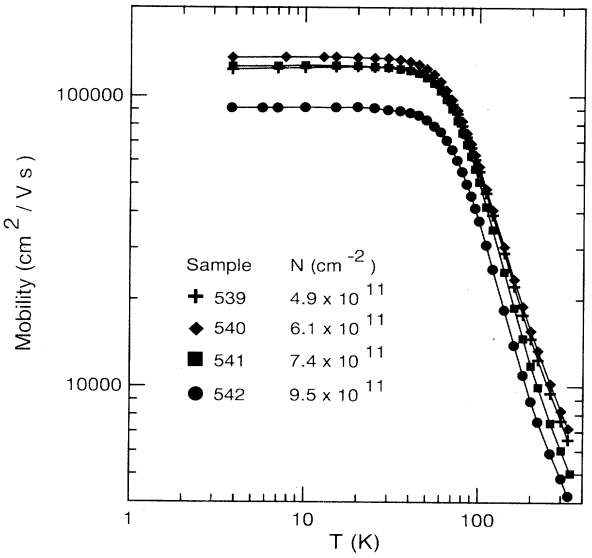

FIG. 1. The temperature dependence of the mobility of the four $In_{1-x}Ga_xAs$ samples used in this study.

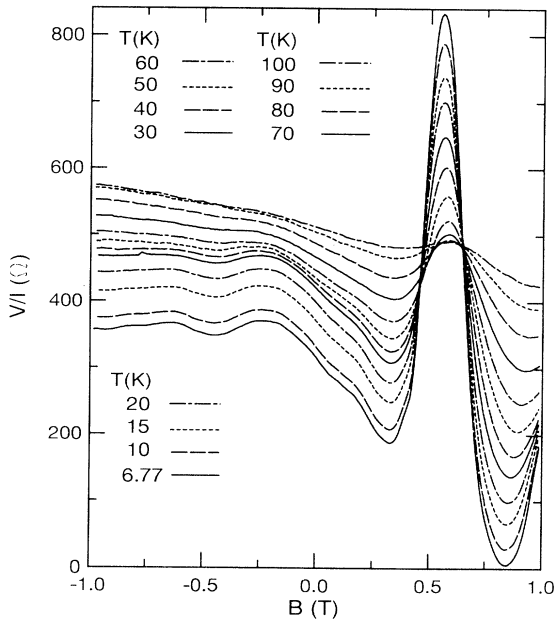

FIG. 2. Magnetic-field dependence of the three-terminal resistance of TEF device 539-2127 built from film 539, at different temperatures. The lowest curve was measured at 6.77 K, and the successive curves from bottom to top correspond to the temperatures shown in the insets.

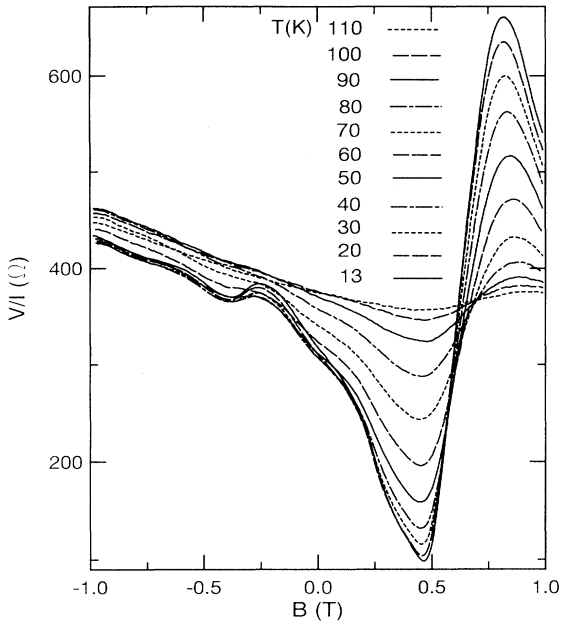

FIG. 3. Magnetic-field dependence of the three-terminal resistance of TEF device 540-2155 built from film 540, at different temperatures. The lowest curve was measured at 13 K, and the successive curves from bottom to top correspond to the temperatures shown in the inset.

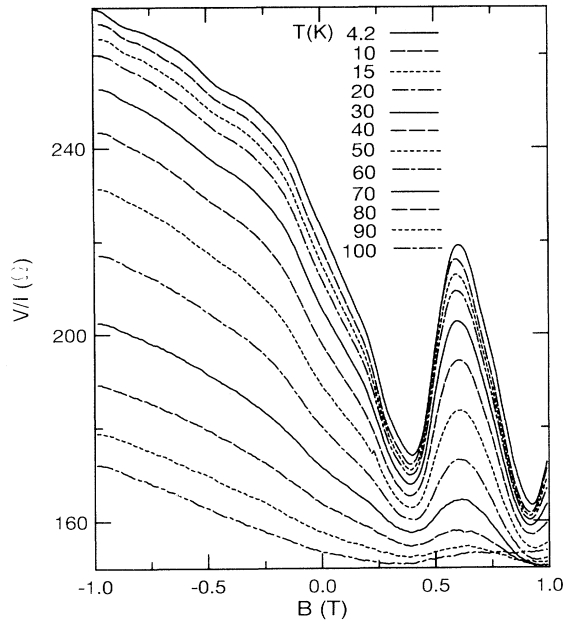

FIG. 4. Magnetic-field dependence of the three-terminal resistance of TEF device 541-2172 built from film 541, at different temperatures. The highest curve was measured at 4.2 K, and the successive curves from top to bottom correspond to the temperatures shown in the inset.

$$B_m L_e = (2\hbar/e)k_F = (2\hbar/e)(2\pi N_a)^{1/2} . \quad (2)$$

From the position of B_m and the densities in Fig. 1, the electrical distance L_e between the contacts can be calculated, and is also given in Table I. The correlation between the geometrical dimension L_g and the calculated L_e is very reasonable, given the uncertainty in the exact geometry of the current distribution in the injector contact, in N_a, and given the effects of the depletion of electrons at the mesa boundaries.

RESULTS AND DISCUSSION

The focusing peak amplitude at the lowest field is defined as the difference between the maximum value seen in Figs. 2–4, and the value at the minimum which occurs in every sample at a field below the focusing peak. This minimum has not been observed in metals,[2,3,9,10] but very often in 2D systems.[5,6,7,11,12] Two other arbitrary definitions of the amplitude have been tried (V/I at maximum minus V/I at $B=0T$, and V/I at low-field minimum minus V/I at $B=-0.25$ T), and yield almost identical temperature dependences. In Figs. 5–7, the amplitudes of the focusing peaks are plotted as a function of temperature.

Even though the main aim of this work is to provide the data reported in Figs. 2–7, we can speculate about the factors affecting the amplitude. The subband level splitting can be estimated to be over 100 meV, using the triangular well approximation. In all samples, therefore, only the last sublevel is populated, which is confirmed by the SdH data. The Fermi energy in the samples is on the order of 20–40 meV, so that, in the temperature range in which focusing is observed, $kT < E_F$. At low tempera-

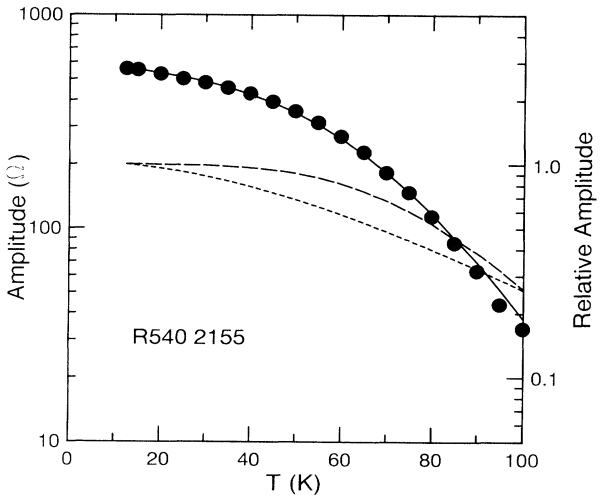

FIG. 5. Temperature dependence of the amplitude of the focusing peak in TEF device 540-2155 (data points, left ordinate). The full line is the fitted amplitude (left ordinate), Eq. (5). The dashed and dotted lines correspond to the right ordinate axis, and represent the relative contributions of the effect of the finite relaxation time (dashes) and of the smearing of the Fermi surface (dots).

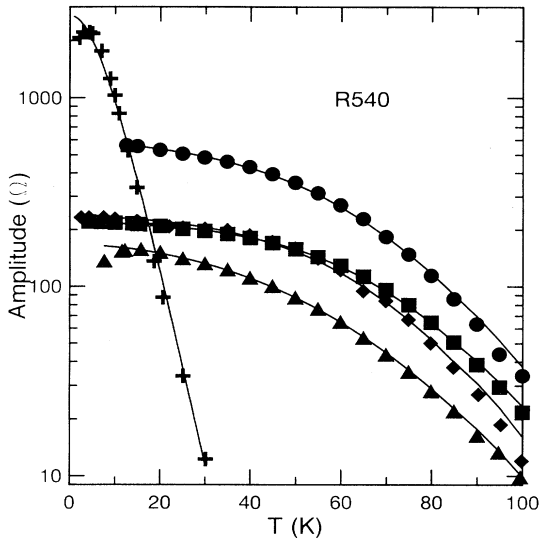

FIG. 6. Temperature dependence of the focusing peak amplitude in four devices made from sample 540 (dots, squares, rhombi, and triangles), and fits using Eq. (5) (lines). The crosses are data points for the amplitude of a Shubnikov–de Haas oscillation at 2.45 T, and the line through them is a fit to them using Eq. (5) using only the Fermi smearing factor, and only one adjustable parameter, the amplitude at $T=0$ K.

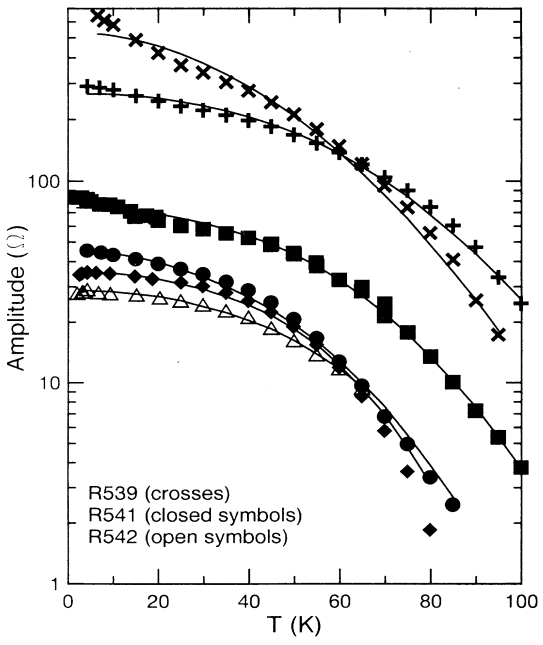

FIG. 7. Temperature dependence of the focusing amplitude in two devices made from sample 539 (symbols + and ×), three devices made from film 541 (dots, squares, and rhombi), and one from film 542 (open triangles). The lines are fits using Eq. (5).

ture, the amplitude of electron focusing in metals[9,10] as well as in semiconductors[11] has been reported to vary with the scattering as

$$V/I=R_0\exp[-(\pi/2)L_e/l_s]\ , \tag{3}$$

where l_s is a characteristic scattering length. This fundamental form was established by varying L_e. In the present work, the change in temperature results in a change of mobility, and, thus, via Eq. (1), of mean free path l_μ. However, it is clear from Fig. 1 that l_μ is temperature independent up to 30 K, while the amplitudes in Figs. 5–7 vary considerably in that temperature range. Equation (3), with l_s proportional to l_μ, does not fit the data. Two factors may explain this observation: the effect of small-angle scattering at low temperature, and the thermal smearing of the Fermi surface. Further experimentation on different mesoscopic device structures and on different material systems is needed to establish the real physical cause of the observations reported here.

The mobility mean free path l_μ, in which each scattering event is attributed a weighing factor $[1-\cos(\theta)]$, where θ is the scattering angle, is in principle different from the scattering length characteristic of electron focusing, l_s, which is more sensitive to small-angle scattering. If the angular dependence of the scattering mechanisms in the samples studied here (presumably mostly ionized impurity scattering, remote impurity scattering, and acoustic-phonon scattering in this temperature range) were known, one could, in principle, calculate the temperature dependence of l_s/l_μ. Alternatively, if further experiments establish that this is the only mechanism, or if the influence of the other mechanisms can be calculated, the data could be used to deduce the temperature dependence of small-angle scattering.

The second possible mechanism is the thermal smearing of the Fermi surface. *A priori,* thermal smearing could be modeled by taking the classical expression for the field dependence of the first focusing peak:[12]

$$V/I=(h/2e^2)\pi/(k_FL_e)\times(L_e/2R_c)^2/[1-(L_e/2R_c)^2]^{1/2}\ , \tag{4}$$

where k_F is the Fermi wave vector and R_c the cyclotron orbit at each field, and convoluting that quantity with the derivative of the Fermi function $(-df/dE)$. This procedure would, however, widen the width of the focusing peaks as their amplitude is decreased, and would keep the area under the peaks constant. Such behavior is not observed experimentally (see Figs. 2 and 4). The temperature dependence of the shape of Shubnikov–de Haas and de Haas–van Alphen oscillations is empirically more similar: the amplitude decreases with temperature, but the nodes of the oscillations are fixed, and their widths thus are nearly temperature independent. The same two factors that contribute to the temperature dependence of the SdH oscillations also contribute to the decay of the amplitude of the focusing peaks: the thermal smearing of the Fermi surface, and the effect of the finite relaxation time τ. Since we are not aware of a theory developed for focusing, we chose to parametrize the influence of these

factors using the Dingle theory developed for the amplitude of the quantum oscillations.[13] The amplitude is described by a factor $R(T)$:

$$R(T)=A[(aT/B)/\sinh(aT/B)]\exp(-b\pi/\omega_c\tau)\ , \tag{5}$$

where A is a scaling factor, the second factor (containing the hyperbolic sine) describes the effect of the thermal smearing of the Fermi surface, and the third factor (the exponential), describes the effect of the finite relaxation rate. Parameter a is related to the effective mass m^* of the carrier via

$$a=2\pi^2 km^*/(e\hbar)\ , \tag{6}$$

if we consider only the first of the possible harmonics that contribute to the SdH oscillations. Parameter b is supposed to be 1 under the same assumption. In the analysis of SdH oscillations, the index p of the harmonic[13] ($p=1,2,\ldots$) of the oscillation equals parameter b, and multiplies parameter a. The physical origin of the attenuation lies in the smearing of the phase of the SdH oscillations when the electron energy levels are broadened. This broadening is due to the effect of the thermal smearing of the Fermi distribution function (the $[(aT/B)/\sinh(aT/B)]$ factor), and to the uncertainty principle which induces a Lorentzian distribution function when the electrons have a finite relaxation time τ (the exponential factor). By varying the temperature, we vary both factors. The width of the Fermi distribution, kT, can be compared to that of the Lorentzian distribution $[\hbar/2\tau]$, and to $[\hbar\omega_c]$ at $B=B_m$ in the relevant temperature range. At 4 K, the energies involved scale as $\hbar/2\tau$ (0.15 meV) for $\mu\approx 100\,000$ cm^2/V s$\approx kT$(0.3 meV)$<\hbar\omega_c$(1 meV at 0.5 T), while, at 100 K, $\hbar/2\tau$(0.3 meV) for $\mu\approx 50\,000$ cm^2/V s$<\hbar\omega_c$(1 meV at 0.5 T)$<kT$(9 meV) (for this comparison, we deduced τ is from the mobility, while in fact it is the single-particle relaxation time). The exponential in Eq. (5) is similar to that in Eq. (3). In Fig. 5, we fitted the amplitude to Eq. (5), using A, a, and b as adjustable parameters and substituting the measured values of μB_m for $\omega_c\tau$. In doing so, we fold the difference between the single-particle relaxation time and the mobility relaxation time, which can be different because of the influence of small-angle scattering, into the fitting parameter b. This assumes that the influence of small-angle scattering is temperature independent, which may not be the case. The results for the parameters are $a=0.027$ T/K and $b=3.5$. The dotted curve in Fig. 5 is the Fermi smearing factor, while the dashed curve is the effect of $\tau(T)$ (the exponential), renormalized to the value at 4.2 K, and shown using the right-hand ordinate scale. While Eq. (5) is simply a way to parametrize the observation, and not a physical explanation, the calculation illustrates that the temperature dependence of the amplitude below 30 K could be attributed to thermal smearing of the Fermi surface, while at $T>35$ K both phonon scattering and Fermi smearing come into play. The same fit was made to the other amplitude versus temperature data points in Figs. 6 and 7, and the resulting parameters are, on average, $a=0.027\pm0.006$ T/K, and $b=3.4\pm1.4$. For comparison, in Fig. 6 we show the decay in amplitude of one SdH oscillation of growth 540 at 2.45 T, which follows Eq. (5): the line through the data points was obtained fitting only one adjustable parameter, the amplitude at 0 K, while the role of the relaxation time was neglected ($b=0$) and the value of a ($a=0.67$ T/K) was calculated from Eq. (6) with $m^*=0.045^*m_e$ (Ref. 14). Similar fits were possible on all extrema of the SdH curves that were resolved over a sufficient temperature range. The value of parameter a is 25 times smaller for the focusing amplitudes than for the SdH oscillations. Because there is no rigorous justification for the use of Eq. (5), we take this simply to reflect the fact that the temperature dependence is much less pronounced in the case of focusing, as seen in Fig. 6. We can speculate that this reduction in temperature dependence reflects the fact that, in the SdH effect, any variation of the cyclotron frequency from the resonant value results in a decay in amplitude through phase smearing, while, in electron focusing, the finite width of the collector and injector contacts permits the collection of electrons that have a wider range of cyclotron radii. No correlation was observed between the values of parameter a obtained on the different TEF devices and the geometrical widths reported in Table I. Though there is a considerable spread in the fitted values of b, it is clear that $b>1$. This is consistent with the observation (11) that l_s is several times smaller than l_μ.

SUMMARY

Electron focusing has been observed in the 2D electron gas at the interface between lattice-matched $In_{1-x}Ga_xAs$ on InP, at temperatures in excess of 100 K, where electron-phonon interactions limit the mean free path. The purpose of this work is to provide experimental curves representing the amplitude of the first focusing peak as a function of temperature. Previous work, in which the temperature was held constant and the device geometry changed, indicates an exponential decay of the focusing peak amplitude with the length of the electron trajectories. This exponential law cannot be extrapolated to predict the decay of the amplitude with increasing temperature, taking into account only the decrease of the mobility. Possible reasons for this are the influence of small-angle scattering, and the thermal smearing of the Fermi surface.

ACKNOWLEDGMENTS

The author acknowledges useful conversations with Professor Ole P. Hansen, Professor W. Zawadzki, and Dr. J. J. Heremans.

[1]Yu. V. Sharvin and L. M. Fischer, Pis'ma Zh. Eksp. Teor. Fiz. **1**, 54 (1965) [JETP Lett. **1**, 152 (1965)].

[2]V. S. Tsoi, Pis'ma Zh. Eksp. Teor. Fiz. **19**, 114 (1974) [JETP Lett. **19**, 70 (1974)].

[3]V. S. Tsoi, J. Bass, and P. Wyder, Adv. Phys. **41**, 365 (1992).

[4]Yu. A. Kolesnichenko, Fiz. Nizk. Temp. **18**, 1059 (1992) [Sov. J. Low Temp. Phys. **18**, 741 (1992)].

[5]H. van Houten, B. J. van Wees, J. E. Mooij, C. W. J. Beenakker, J. G. Williamson, and C. T. Foxon, Europhys. Lett. **5**, 721 (1988); for a review, see C. W. J. Beenakker and H. van Houten, in *Solid State Physics,* edited by H. Ehrenreich and D. Turnbull (Academic, New York, 1991), Vol. 44.

[6]J. Spector, H. L. Stormer, K. W. Baldwin, L. N. Pfeiffer, and K. W. West, Appl. Phys. Lett. **56**, 967 (1990); see also related work by the same authors in Appl. Phys. Lett. **56**, 1290 (1990); **56**, 2433 (1990); **58**, 263 (1991).

[7]J. J. Heremans, M. B. Santos, and M. Shayegan, Appl. Phys. Lett. **61**, 1652 (1992).

[8]V. S. Tsoi, Pis'ma Zh. Eksp. Teor. Fiz. **22**, 409 (1975) [JETP Lett. **22**, 197 (1975)].

[9]P. C. van Son, H. van Kempen, and P. Wyder, Phys. Rev. Lett. **58**, 1567 (1987).

[10]P. A. M. Benistant, G. F. A. van de Walle, H. van Kempen, and P. Wyder, Phys. Rev. B **33**, 690 (1986).

[11]J. Spector, H. L. Stormer, K. W. Baldwin, L. N. Pfeiffer, and K. W. West, Surf. Sci. **228**, 283 (1990).

[12]H. van Houten, C. W. J. Beenakker, J. G. Williamson, M. E. I. Broekaart, P. H. M. van Loosdecht, B. J. van Wees, J. E. Mooij, C. T. Foxon, and J. J. Harris, Phys. Rev. B **39**, 8556 (1989).

[13]D. Schoenberg, *Magnetic Oscillations in Metals* (Cambridge University Press, Cambridge, 1984).

[14]*Semiconductors. Physics of Group IV Elements and III-V Compounds,* edited by O. Madelung, M. Schulz, and H. Weiss, Landolt-Bornstein, New Series, Group III, Vol. 17, Pt. a (Springer-Verlag, Berlin, 1982).